Analytic Model for Acoustic Propagation in the Deep Sound Channel

William H. Press
University of Texas at Austin

November 9, 2013

Introduction

In the deep ocean, when the subsurface sound velocity profile has a minimum at some depth, there is a deep sound channel that allows long-distance acoustic propagation. Within a range of angles around the horizontal, rays launched within the sound channel are refracted in such a way as to remain within the channel, neither intersecting the ocean surface nor (for a sufficiently deep ocean) the bottom.

While it is not difficult, for any given sound velocity profile $v(z)$, to trace the sound rays by numerical solution of ODEs, such solutions are inconvenient for developing an intuitive understanding of the associated phenomena. We here derive an analytic model that, while not exact, furthers such understanding.

Derivation of the Analytic Model

We first derive Snell's law in the standard way. Consider a small vertical section, height Δz, of an acoustical wavefront propagating locally in the $+x$ direction. Suppose that the sound velocity is v_1 at the bottom of the segment and v_2 at the top of the segment. Then after time Δt, the bottom of the front has advanced a distance $v_1 \Delta t$, while the top has advanced $v_2 \Delta t$, introducing a change in slope of $(v_2 - v_1)\Delta t/\Delta z = \Delta v \Delta t/\Delta z$ over a distance $v\Delta t$. So, in the limit, we have for the change in the ray direction from horizontal,

$$\frac{d\theta}{dx} = -\frac{1}{v}\frac{dv}{dz} = -\frac{d\log v}{dz} \tag{1}$$

When we apply this to rays other than horizontal, we are making a small-angle approximation, and we do this henceforth.

Equation (1) when paired, again in small angle approximation, to the geometrical equation

$$\frac{dz}{dx} = \theta \tag{2}$$

gives the ray-tracing equation

$$\frac{d^2z}{dx^2} = -\frac{d}{dz}\log v(z) \tag{3}$$

This is the equation of an undamped anharmonic oscillator with potential $\log v(z)$. Any profile $v(z)$ with a minimum thus implies the existence of rays whose depth oscillates between an upper and a lower turning point. Because the equation is undamped, there is a conserved "energy"

$$E(x) = \frac{1}{2}\left(\frac{dz}{dx}\right)^2 + \log v(z) = \text{constant} \tag{4}$$

along every ray. In particular, a ray launched horizontally at any depth will return to that same depth at a subsequent turning point.

Harmonic Case

It is convenient first to consider the unrealistic case where the oscillator is exactly harmonic, that is, the case where $\log v(z)$ is exactly a parabola. Then, if P is the period of the harmonic oscillator, the general solution is a linear combination of $\sin(2\pi x/P)$ and $\cos(2\pi x/P)$. In particular, the solution for a ray launched at depth z_0 with slope $z_0' \equiv dz/dx$ is

$$z(x) = z_0\cos(2\pi x/P) + z_0'\sin(2\pi x/P) \tag{5}$$

Although we might loosely call the z coordinate "depth", we are measuring it upward from the location of the velocity minimum (the axis of the sound channel), not downward from the surface. Equation (5) implies that the amplitude A of $z(x)$, measured from the velocity minimum upwards to any upper turning point, is

$$A = (z_0^2 + {z_0'}^2)^{1/2} \tag{6}$$

Exactly those rays with amplitudes A less than the depth of the velocity minimum do not intersect the surface. It is thus convenient to measure

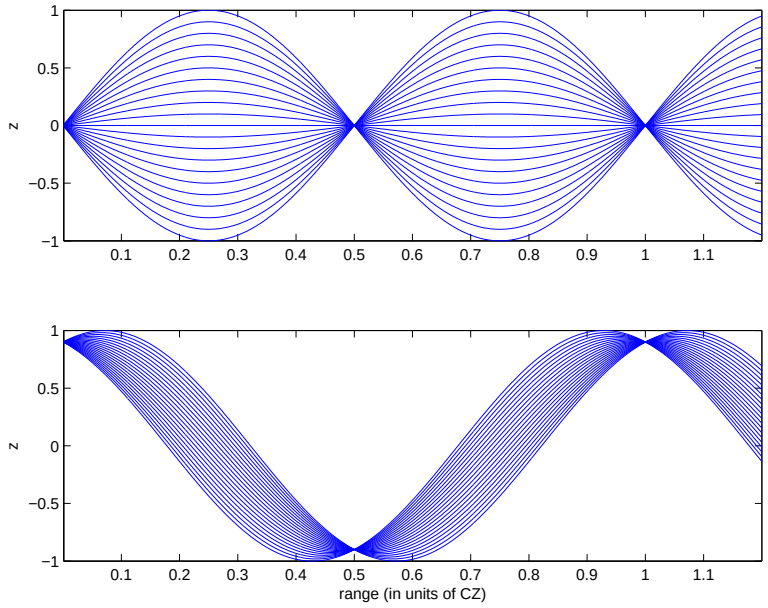

Figure 1: Acoustic rays traced from two different depths, showing all angles that remain in the sound channel (do not intersect the surface). Shown is the unrealistic case of an harmonic potential. Top: launched from the center of the sound channel. Bottom: launched from a depth 0.1 of the sound channel center depth (that is, $z = 0.9$).

vertical distance in units of the depth of the velocity minimum. Then, at any vertical position z_0 rays launched with angles (slopes) satisfying

$$-\sqrt{1 - z_0^2} < z_0' < \sqrt{1 - z_0^2} \tag{7}$$

will not intersect the surface. In other words, from any position z_0, equation (7) defines our angular "window" into the sound channel. It is convenient for us, henceforth, to measure angles in units of $(1 - z_0^2)^{1/2}$, so that our window extends, in these units, from -1 to $+1$. Similarly, it is convenient to scale horizontal distances in units of the period P, which is the distance to the first convergence zone (CZ).

With these scaling conventions, Figure 1 shows rays that fill the sound channel window as launched from two different depths, first from the center of the sound channel (depth of the velocity minimum), and second from a shallower $z = 0.9$ (i.e., depth 0.1 times the velocity minimum depth).

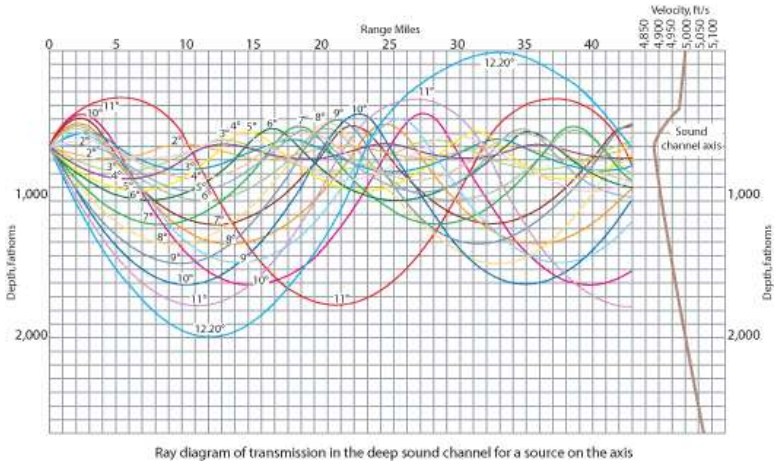

Figure 2: Ray diagram of transmission in the deep sound channel for a source on the axis (after Whitman).

Anharmonic Case

In the bottom diagram of Figure 1, we are particularly interested in rays near the first convergence zone, around $x = 1$. What is notably unrealistic about the harmonic case, and Figure 1, is that the rays return to a perfect focus. This is a property of harmonic oscillators, but not of the general anharmonic potential $\log v(z)$. A key property of anharmonic oscillators is that their period P depends on their amplitude A. We need to capture this in our model. Expressing the relation as a Taylor series, by analyticity (or symmetry) the linear term must be absent, so

$$P = P_0(1 + \text{coefficient} \times A^2 + \ldots) \approx P_0[1 + \alpha(z_0^2 + {z'_0}^2)]/(1 + \alpha) \qquad (8)$$

Here the approximation sign means that we are going to neglect all terms except the lowest order one, in A^2. The denominator factor $1 + \alpha$ is chosen to make P_0 the period of the surface-tangent wave. Our model thus has a single empirical parameter, α.

Figure 2, from a U.S. Navy popular article [1], shows a more realistic set of ray traces from the center of a notional sound channel. One sees that rays launched nearly horizontally (that is, with small amplitude) have a period of about 1/3 of that of the ray that just touches the surface. So, for the numerical results shown below, we take $\alpha = 2$ as an illustrative approximation.

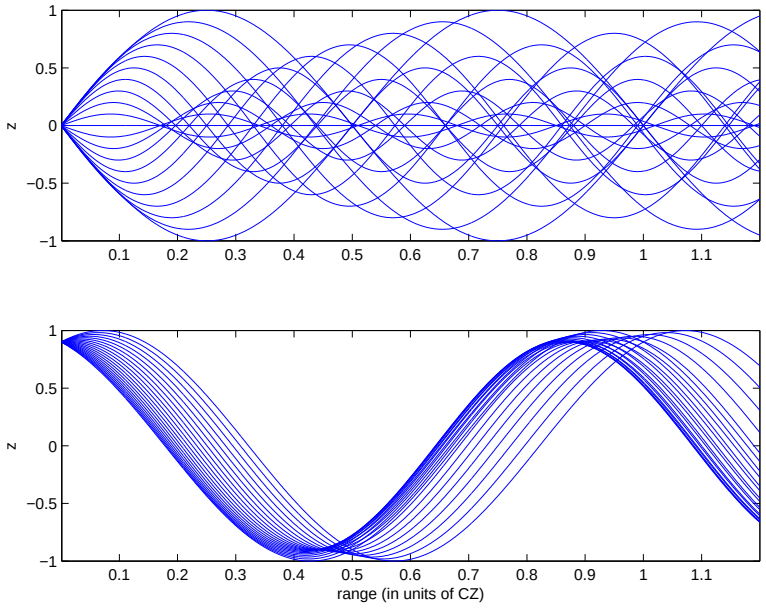

Figure 3: Same as Figure 1, but with anharmonicity introduced by the period-amplitude relation of equation (8). The top figure is in qualitative agreement with Figure 2's "data". (Note that Figure 2 does not plot a complete set of positive and negative angles.)

Figure 3 shows ray propagation for our adopted anharmonic model, namely equations (5) and (8) (with $P_0 \equiv 1$). When our interest is in rays launched and received relatively close to the surface (that is, at a small fraction of the depth of the sound channel axis, as in Figure 3 bottom), then the adjustable model parameter α controls the spread in range of the surface tangent rays in the convergence zone around $x = 1$. We could in principle improve the fidelity of the model by adding a parameter β to control the concavity (second derivative) of these tangencies. (The simplest way to do this would be by a β-dependent reparameterization of z near the surface.) These two parameters, α and (notionally) β capture almost everything that is observable about the sound channel by shallow observations. That is, sound channels with quite different velocity profiles at depth, but which happen to have the same values α and β, should be nearly indistinguishable.

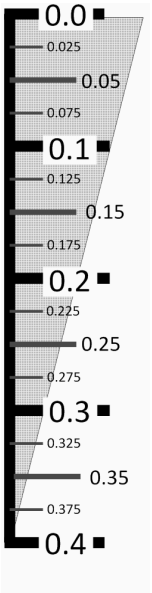

Figure 4: Plimsoll "target" extending from the sea surface (labeled 0.0) down to a depth 0.4 of the distance to the sound channel axis (labeled 0.4). We can image this target acoustically at various ranges by mapping the angle of rays from our position to their intersection with the target at range, thus illustrating topological properties of the acoustic field in the sound channel.

Acoustic "Images"

One way to gain intuition about the acoustic effects of complicated ray paths is to imagine that we can acoustically image a target at various distances. We are at some depth z_0, and (with the scaling mentioned above), our acoustic image of the sound channel consists of incoming rays at angles $0 \leq z_0' \leq 1$. Imagine a fiducial "target", such as that shown in Figure 4, suspended from the sea surface – as if the underwater plimsoll on the side of a ship with very deep draft! (In the Figure, the plimsoll extends to a depth 0.4 of the sound channel axis.)

As we move a fiducial target out in distance (Figure 5), we first see the target disappearing ($x = 0.15$) as rays from the receiver position are bent down to below the target's bottom. Approaching the convergence zone, two images of the target, from its bottom, appear and expand ($x = 0.77$). By $x = 0.88$ further splitting has occurred – note the high magnification (and

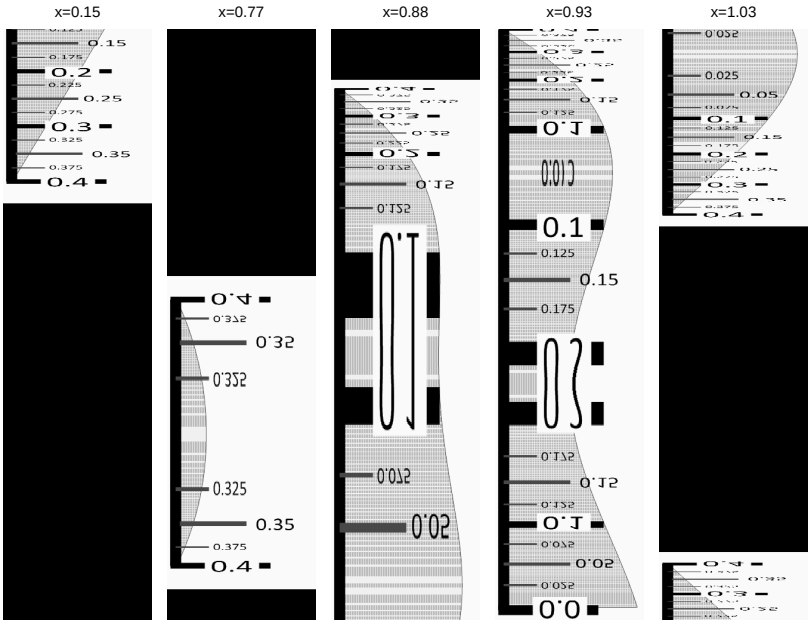

Figure 5: Acoustic images of the target in Figure 4 at various ranges. From left to right: $x = 0.15, 0.77, 0.88, 0.93$, and 1.03. The range of the CZ is nominally $x = 1$ in these units.

therefore large acoustic intensity) from a target position at the same depth as the receiver. By $x = 0.93$ there is pronounced further splitting, with thee images of some depths (e.g., depth 0.1). Finally, beyond the convergence zone, the two remaining images begin to disappear, one off the top, the other off the bottom.

The above description, and Figure 5, become much clearer in the movie, which can be viewed on YouTube at `http://youtu.be/Q9hAmVLb8KY`

Topology of the Images

Figure 6 shows a different view of the same simulation as shown in Figure 5. The lower panel shows a magnified view of the rays around the convergence zone. The receiver (far left of the figure, at $x = 0$) is at the depth shown as a green horizontal line. The upper panel shows, as a function of range on the same scale, the angle of arrival at the receiver of rays emitted from various depths, labeled on the contour lines in the figure.

One sees that, for all emitted depths, images first appear with increasing range in pairs, then often bifurcate so that as many as three images can be present together. Note that there is no continuation of the curves above or below the angle of arrivals interval shown: outside of the range shown, rays are not confined to the sound channel, but intersect the sea surface.

Also note that there are two topologically distinct classes of images, depending on whether the source is above or below the receiver in depth. For sources below the receiver, as a function of increasing range (red contours), the second and third images appear by bifurcation *below* a single surviving upper image, after the original lower image has disappeared. For sources above the receiver (blue contours), the second and third images bifurcate *above* a remaining upper image.

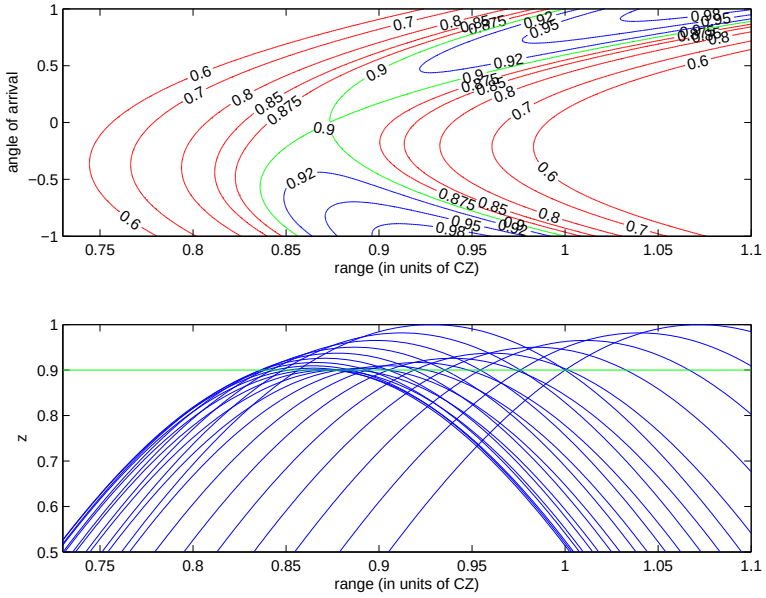

Figure 6: Visibility of targets at various depths as a function of range from receiver. The receiver is assumed to be at $z = 0.9$. (The surface is at $z = 1$.) A target is visible when a vertical line in the top figure intersects its labeled contour. It has multiple images when, as is usually the case, there is more than one such intersection. One sees topologically distinct behaviors for targets above the receive depth ($z > 0.9$) versus below the receiver depth ($z < 0.9$).

References

[1] Edward C. Whitman, "SOSUS: The Secret Weapon of Undersea Surveillance", *Undersea Warfare*, vol. 7, no. 2 (Winter, 2005) at http://www.navy.mil/navydata/cno/n87/usw/issue_25/sosus.htm